Integrin $\alpha_v\beta_6$–Targeted SPECT Imaging for Pancreatic Cancer Detection

Zhaofei Liu*[,1,2], Hao Liu*[,1,2], Teng Ma[1,2], Xianlei Sun[1,2], Jiyun Shi[1], Bing Jia[1,2], Yi Sun[3], Jun Zhan[4,5], Hongquan Zhang[4,5], Zhaohui Zhu[3], and Fan Wang[1,2,6]

[1]Medical Isotopes Research Center, Peking University, Beijing, China; [2]Department of Radiation Medicine, School of Basic Medical Sciences, Peking University, Beijing, China; [3]Department of Nuclear Medicine, Peking Union Medical College Hospital, Beijing, China; [4]Key Laboratory of Carcinogenesis and Translational Research, Ministry of Education, Beijing, China; [5]Laboratory of Molecular Cell Biology and Tumor Biology, Department of Anatomy, Histology and Embryology, Peking University Health Science Center, Beijing, China; and [6]Interdisciplinary Laboratory, Institute of Biophysics, Chinese Academy of Sciences, Beijing, China

Integrin $\alpha_v\beta_6$, a member of the integrin family, is specifically expressed in many malignancies but not in normal organs. Overexpression of integrin $\alpha_v\beta_6$ is usually correlated with malignant potential and poor prognosis. In this study, we describe the synthesis and evaluation of a ^{99m}Tc-labeled integrin $\alpha_v\beta_6$–targeting peptide as a SPECT radiotracer for the in vivo imaging of integrin $\alpha_v\beta_6$ expression. **Methods:** An integrin $\alpha_v\beta_6$–targeting peptide (denoted as the HK peptide) was conjugated with 6-hydrazinonicotinyl (HYNIC) and radiolabeled with ^{99m}Tc using tricine and TPPTS (trisodium triphenylphosphine-3,3′,3″-trisulfonate) as coligands. The in vitro and in vivo characteristics of ^{99m}Tc-HYNIC(tricine)(TPPTS)-HK (^{99m}Tc-HHK) were investigated in BxPC-3 (integrin $\alpha_v\beta_6$–positive) and HEK293 (integrin $\alpha_v\beta_6$–negative) models. The ability of ^{99m}Tc-HHK to detect liver metastasis of pancreatic cancer was evaluated using small-animal SPECT/CT. **Results:** ^{99m}Tc-HHK showed high integrin $\alpha_v\beta_6$–binding specificity both in vitro and in vivo. ^{99m}Tc-HHK was cleared rapidly from the blood and normal organs except for the kidneys. The highest uptake (0.88 ± 0.12 percentage injected dose per gram) of ^{99m}Tc-HHK in BxPC-3 tumors was observed at 0.5 h after injection. High-contrast images of integrin $\alpha_v\beta_6$–positive tumors were obtained using ^{99m}Tc-HHK. The minimum nonspecific activity accumulation in normal liver tissues rendered high-quality SPECT/CT images of metastatic lesions. **Conclusion:** ^{99m}Tc-HHK is a promising SPECT radiotracer for the noninvasive imaging of integrin $\alpha_v\beta_6$ expression in vivo. SPECT/CT with ^{99m}Tc-HHK could provide an effective approach for the noninvasive detection of primary and metastatic lesions of integrin $\alpha_v\beta_6$–positive tumors.

Key Words: pancreatic cancer; molecular imaging; integrin $\alpha_v\beta_6$; phage display; SPECT/CT

J Nucl Med 2014; 55:989–994
DOI: 10.2967/jnumed.113.132969

Pancreatic cancer is one of the most deadly cancers, ranking as the fourth leading cause of cancer-related deaths in the United States (*1*). Most pancreatic cancer patients are diagnosed with advanced stages of this disease, for which curative operation is not a suitable treatment option. Given that the 5-y survival rate after diagnosis is generally below 5% (*2*), the best approach for improving the odds of curing or controlling pancreatic cancer involves early detection and accurate staging.

Advances in molecular imaging techniques have provided numerous opportunities for making earlier and more accurate diagnosis, determining the staging information of various cancers, and monitoring their treatment responses. The development of molecular imaging agents that target specific tumor markers could provide more sensitive and more specific cancer detection. Integrin $\alpha_v\beta_6$, a member of the integrin protein family, is overexpressed in numerous types of carcinomas, such as colon, lung, cervical, ovarian, and pancreatic cancers, but is expressed at low or undetectable levels in healthy organs (*3*). Pancreatic ductal adenocarcinomas exhibit the highest integrin $\alpha_v\beta_6$ expression among gastroenteropancreatic adenocarcinomas (*4*). Moreover, the high expression of integrin $\alpha_v\beta_6$ in carcinomas is a prognostic factor of the disease and is correlated with poor patient survival (*5,6*). Thus, molecular imaging agents that target integrin $\alpha_v\beta_6$ would be highly useful in the receptor-targeted detection of pancreatic cancer and in the noninvasive monitoring of tumor prognosis.

Pioneering studies have recently been conducted on the development of PET radiotracers for in vivo integrin $\alpha_v\beta_6$ imaging (*7–10*). Hausner et al. (*7*) prepared an ^{18}F-radiolabeled 20-mer integrin $\alpha_v\beta_6$–targeting peptide (^{18}F-FBA-A20FMDV2) using a sequence derived from the G-H loop of an envelope protein of the foot-and-mouth disease virus. ^{18}F-FBA-A20FMDV2 exhibited specific integrin $\alpha_v\beta_6$ targeting in vivo. However, low tumor uptake and poor tumor retention limit the general application of this peptide. To increase the tumor uptake and improve the pharmacokinetics of ^{18}F-FBA-A20FMDV2, 2 new radiotracers with polyethylene glycol (PEG) spacers were developed. Small-animal PET imaging results revealed that the modified compounds show significantly improved tumor retention (*8*). Kimura et al. engineered several highly stable cysteine knot peptides, and the ^{64}Cu- (*9*) and ^{18}F- (*10*) labeled compounds proved to be potentially useful for the PET imaging of integrin $\alpha_v\beta_6$.

Although ^{18}F-FDG has been widely used in clinical settings, several drawbacks are associated with ^{18}F-labeled peptide radiotracers. For

Received Sep. 20, 2013; revision accepted Feb. 14, 2014.
For correspondence contact either of the following:
Zhaofei Liu, Medical Isotopes Research Center, Peking University, 38 Xueyuan Rd., Beijing 100191, China.
E-mail: liuzf@bjmu.edu.cn
Fan Wang, Medical Isotopes Research Center, Peking University, 38 Xueyuan Rd., Beijing 100191, China.
E-mail: wangfan@bjmu.edu.cn
*Contributed equally to this work.
Published online Apr. 7, 2014.

example, ^{18}F labeling of peptides typically requires an in-house cyclotron system, a complex infrastructure, and a time-consuming synthesis procedure and tedious postlabeling purification. ^{64}Cu-labeled peptides have been extensively investigated for PET imaging in animal models. However, studies on the clinical application of ^{64}Cu-based radiotracers are limited. In addition, ^{64}Cu-DOTA conjugates generally exhibit high liver accumulation because of the possible dissociation of ^{64}Cu from the chelator (*11*). Compared with PET radiotracers, ^{99m}Tc-labeled SPECT tracers have attracted increased attention because of their high availability and low cost. The high labeling yield of ^{99m}Tc chelator systems allows the formulation of kits for the rapid preparation of radiotracers for nuclear medicine applications. ^{99m}Tc labeling can be accomplished by simply adding $^{99m}TcO_4^-$ to a freeze-dried formulation kit with or without short-period heating (*12*). In this respect, we are particularly interested in the development of ^{99m}Tc-labeled SPECT radiotracers.

Using a phage display approach, the Brown group at University of Texas Southwestern Medical Center isolated a 20-mer peptide from a panning peptide library on the lung adenocarcinoma cell line H2009 (*13*). The peptide, called TP H2009.1, has the sequence RGDLATLRQLAQEDGVVGVR. In subsequent studies, TP H2009.1 was shown to deliver a chemotherapeutic agent specifically to tumor cells in vitro by targeting integrin $\alpha_v\beta_6$ (*14,15*). Previous reports suggested that TP H2009.1 has high potential application in the imaging of integrin $\alpha_v\beta_6$–positive tumors in vivo.

In this study, we designed a peptide sequence, RGDLATLRQLAQEDGVVGVRK (denoted as the HK peptide; H means TP H2009.1), by adding a lysine (K) residue to the TP H2009.1 peptide to provide a C-terminal NH_2 group for chelator conjugation. The HK peptide was conjugated with 6-hydrazinonicotinyl (HYNIC) and then radiolabeled with ^{99m}Tc. The resulting radiotracer RGDLATLRQLAQEDGVVGVRK-HYNIC(tricine)(TPPTS)-^{99m}Tc (^{99m}Tc-HHK; Supplemental Fig. 1 [supplemental materials are available at http://jnm.snmjournals.org]) was evaluated both in vitro and in vivo as a SPECT radiotracer for the in vivo imaging of integrin $\alpha_v\beta_6$–positive pancreatic cancer.

MATERIALS AND METHODS

General

The peptides Fmoc-RGDLATLRQLAQEDGVVGVRK (Fmoc-HK), RGDLATLRQLAQEDGVVGVRYK (HYK), and a scrambled peptide RATGLRQALDQEDGLVVGVRK were synthesized by ChinaPeptides Co., Ltd. The reversed-phase high-performance liquid chromatography (HPLC) system was the same as previously reported (*16,17*).

Preparation of ^{99m}Tc-HHK

Detailed procedures for HYNIC conjugation of the HK peptide are described in the Supplemental "Materials and Methods" section. HYNIC-conjugated HK peptide (HHK) was labeled with ^{99m}Tc using tricine and trisodium triphenylphosphine-3,3′,3″-trisulfonate (TPPTS) as the coligands and then purified with Sep-Pak C18 cartridges (Waters) as previously described (*16*). After purification, the radiochemical purity of ^{99m}Tc-HHK was determined to be more than 98% as analyzed by radio-HPLC.

Cell Culture and Animal Models

The BxPC-3 human pancreatic cancer cell line was obtained from American Type Culture Collection. Human embryonic kidney HEK293 cells were kindly provided by Professor Tao Xu (Institute of Biophysics, China Academy of Science). BxPC-3 cells were grown in RPMI-1640 medium, and HEK293 cells were grown in high-glucose Dulbecco modified Eagle medium. Both cell lines were cultured in medium supplemented with 10% fetal bovine serum at 37°C in humidified atmosphere containing 5% CO_2.

All animal experiments were performed in accordance with the guidelines of Peking University Animal Care and Use Committee. To obtain BxPC-3 and HEK293 subcutaneous tumor models, BxPC-3 cells (1×10^7 in 100 μL of phosphate-buffered saline) or HEK293 cells (5×10^6 in 100 μL of phosphate-buffered saline) were inoculated subcutaneously into the right front flanks of female BALB/c nude mice. The animals were used for in vivo studies when the tumor size reached 200–300 mm^3 (3–4 wk after inoculation). A mouse model of liver metastasis (*18*) was established by direct intrahepatic injection of 1×10^7 BxPC-3 cells (in 50 μL of phosphate-buffered saline) in female BALB/c nude mice. The mice were used for small-animal imaging studies 25 d after cell injection (based on pilot data).

In Vitro Integrin $\alpha_v\beta_6$ Specificity

The expression status of integrin $\alpha_v\beta_6$ in BxPC-3 and HEK293 cells was tested by fluorescence-activated cell sorting analysis as described in the Supplemental "Materials and Methods" section.

The in vitro integrin $\alpha_v\beta_6$–binding affinity and specificity of the HK peptide and its HYNIC-conjugate (HHK) were assessed via a cellular displacement assay using ^{125}I-HYK as the integrin $\alpha_v\beta_6$–specific radioligand. ^{125}I-HYK was prepared by labeling HYK with $Na^{125}I$ using the IODO-GEN (Sigma) method (*19*). The experiments were performed on BxPC-3 cells (integrin $\alpha_v\beta_6$–positive) using a previously described method (*16*). The best-fit 50% inhibitory concentration (IC_{50}) values were calculated by fitting the data with nonlinear regression using Prism software (version 4.0; GraphPad Software).

The integrin $\alpha_v\beta_6$–binding specificity of ^{99m}Tc-HHK was tested using BxPC-3 (integrin $\alpha_v\beta_6$–positive) and HEK293 (integrin $\alpha_v\beta_6$–negative) cells. About 5.55 kBq of ^{99m}Tc-HHK were added to cells grown in 6-well plates with or without an excess amount (5 μg) of the cold HK peptide. After incubation at 4°C for 2 h, the cells were washed and collected. Cell-associated radioactivity was measured using a γ counter. Results were expressed as a percentage of the total added dose per 10^5 cells.

Biodistribution

Female nude mice bearing BxPC-3 or HEK293 tumor xenografts were injected with 0.37 MBq of ^{99m}Tc-HHK to evaluate the distribution of this radiotracer in tumor tissues and major organs ($n = 4$ per group). The mice were sacrificed and dissected at 0.5, 1, 2, and 4 h after injection. Blood, tumor, major organs, and tissues were collected and weighed. The radioactivity in the tissue was measured using a γ counter. The results are presented as percentage injected dose per gram of tissue (%ID/g). Two blocking studies were also performed in 8 nude mice bearing BxPC-3 tumor xenografts ($n = 4$ mice per group). For the HK peptide–blocking group, each mouse was coinjected with 500 μg of unlabeled HK peptide and 0.37 MBq of ^{99m}Tc-HHK. For the scrambled peptide–blocking group, each mouse was coinjected with 500 μg of the scrambled peptide (RATGLRQALDQEDGLVVGVRK) and 0.37 MBq of ^{99m}Tc-HHK. At 1 h after injection, all mice were sacrificed, and organ biodistribution of ^{99m}Tc-HHK was determined.

Planar γ and Small-Animal PET Imaging

Each BxPC-3 or HEK293 tumor–bearing nude mouse was injected via the tail vein with 18.5 MBq of ^{99m}Tc-HHK ($n = 4$ per group). A blocking study was also performed in 4 BxPC-3–bearing mice by coinjecting 18.5 MBq of ^{99m}Tc-HHK with an excess dose (500 μg) of the HK peptide. Animals were placed prone on a 2-head γ camera (Millennium VG; GE Healthcare) equipped with a parallel-hole, low-energy, and high-resolution collimator. Planar images were acquired at 1 h after injection and stored digitally in a 128 × 128 matrix.

PET scans and image analysis were performed using a microPET R4 rodent model scanner (Siemens Medical Solutions). Each BxPC-3 or HEK293 tumor–bearing nude mouse was injected via the tail vein with 3.7 MBq of ^{18}F-FDG under 2% isoflurane anesthesia ($n = 4$ per group). Five-minute static PET scans were acquired at 1 h after injection, and the region-of-interests–derived %ID/g values were calculated as previously described (*17*). As a control experiment, 3.7 MBq of ^{18}F-FDG was coinjected with 500 μg of the cold HK peptide into a group of 4 BxPC-3–bearing mice, and small-animal PET scans were then obtained.

Small-Animal SPECT/CT Imaging

Small-animal SPECT/CT scans of the BxPC-3 mouse model of liver metastasis were obtained using a NanoSPECT/CT tomograph (Bioscan Inc.) as previously described (*17*). Briefly, each mouse was injected via the tail vein with 37 MBq of ^{99m}Tc-HHK. At 1 h after injection, the mice were anesthetized by inhalation of 2% isoflurane and imaged using the NanoSPECT/CT camera. The SPECT and CT fusion images were obtained using the automatic fusion feature of the InVivoScope program (Bioscan Inc.). After SPECT/CT imaging, BxPC-3 mice with liver metastasis were sacrificed. Livers were excised and macroscopically surveyed to detect tumor lesions. For further confirmation of the tumor lesions, metastatic liver lesions were fixed in 5% buffered formalin, embedded in paraffin, cut into sections, and then subjected to hematoxylin and eosin (H&E) staining.

Statistical Analysis

Quantitative data were expressed as mean ± SD. Means were compared using the Student *t* test. *P* values of less than 0.05 were considered statistically significant.

RESULTS

Chemistry and Radiochemistry

Fmoc-HK-HYNIC was prepared by direct conjugation of Fmoc-HK peptide with HYNIC-NHS. After the removal of the Fmoc group, the final product HK-HYNIC (HHK) was confirmed by HPLC and mass spectrometry. The ^{99m}Tc-labeling procedure was done within 30 min, with a yield of 94.8% ± 1.1% ($n = 16$). The radiochemical purity was greater than 98%, and the specific activity of ^{99m}Tc-HHK (Supplemental Fig. 1) was greater than 180 GBq/μmol.

In Vitro Integrin $\alpha_v\beta_6$ Specificity

Fluorescence-activated cell sorting analysis clearly showed that BxPC-3 tumor cells were integrin $\alpha_v\beta_6$–positive, whereas HEK293 cells were integrin $\alpha_v\beta_6$–negative (Fig. 1A). Both HK and HHK inhibited the binding of ^{125}I-HYK to integrin $\alpha_v\beta_6$–expressing BxPC-3 cells in a concentration-dependent manner. The IC_{50} values for HK and HHK were 2.16 ± 0.11 and 2.72 ± 0.15 nM, respectively (Fig. 1B).

We also investigated the cell-binding properties of ^{99m}Tc-HHK in both integrin $\alpha_v\beta_6$–positive BxPC-3 and integrin $\alpha_v\beta_6$–negative HEK293 cells. As shown in Figure 1C, the binding values (percentage of the total added dose per 10^5 cells) of ^{99m}Tc-HHK for BxPC-3 and HEK293 cells were 4.90 ± 0.31 and 0.18 ± 0.05, respectively ($P < 0.001$). The binding of ^{99m}Tc-HHK to BxPC-3 cells was significantly inhibited by the addition of an excess dose of the HK peptide (from 4.90 ± 0.31 to 0.09 ± 0.01, $P < 0.001$).

Biodistribution

As shown in Figure 2A, the uptake values of ^{99m}Tc-HHK in BxPC-3 tumors were 0.88 ± 0.12, 0.52 ± 0.03, 0.36 ± 0.06, and 0.32 ± 0.04 %ID/g at 0.5, 1, 2, and 4 h after injection, respectively. The tumor uptake of ^{99m}Tc-HHK was significantly higher than that in the blood and normal organs, such as the heart, pancreas, bone, and muscle, at almost all time points examined ($P < 0.05$).

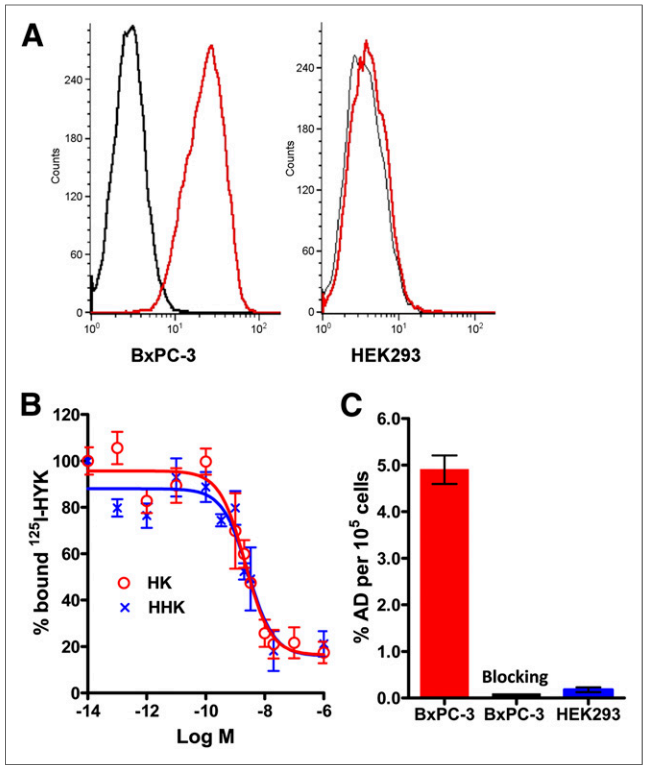

FIGURE 1. (A) Representative flow cytometry histograms of BxPC-3 and HEK293 cells without (black-outlined spectrum) and with (red-outlined spectrum) addition of antiintegrin $\alpha_v\beta_3$ antibody. (B) Inhibition of ^{125}I-HYK binding to integrin $\alpha_v\beta_6$ on BxPC-3 cells by HK and HHK peptides. (C) Binding of ^{99m}Tc-HHK to BxPC-3 (without or with 5 μg of HK peptide blocking) and HEK293 cells. %AD/10^5 cells = percentage of total added dose per 10^5 cells.

^{99m}Tc-HHK showed similar biodistribution patterns in the normal organs of integrin $\alpha_v\beta_6$–negative HEK293 mice, compared with those in integrin $\alpha_v\beta_6$–positive BxPC-3 tumor–bearing mice (Fig. 2B). However, the uptake of ^{99m}Tc-HHK in BxPC-3 tumors was significantly higher than that in HEK293 tumors (0.88 ± 0.12 vs. 0.32 ± 0.07 %ID/g, $P < 0.01$, and 0.52 ± 0.03 vs. 0.16 ± 0.03 %ID/g, $P < 0.001$, at 0.5 and 1 h after injection, respectively). The coinjection of an excess dose of the cold HK peptide with ^{99m}Tc-HHK resulted in a significantly reduced tumor uptake at 1 h after injection (from 0.52 ± 0.03 to 0.28 ± 0.08 %ID/g, $n = 4$, $P < 0.01$). In contrast, the coinjection of an excess dose of a scrambled peptide with ^{99m}Tc-HHK did not reduce the tumor uptake (0.52 ± 0.03 vs. 0.60 ± 0.17 %ID/g, $n = 4$, $P > 0.05$; Fig. 2B).

Planar γ Imaging and Small-Animal PET Imaging

Three groups of tumor-bearing mice (BxPC-3, BxPC-3/HK blocking, and HEK293) were subjected to both ^{99m}Tc-HHK and ^{18}F-FDG imaging at 1 h after injection. As shown in Figure 3A, the BxPC-3 tumor was clearly visible, with high contrast in relation to the contralateral background after ^{99m}Tc-HHK injection. The tumor-to-blood and tumor-to-muscle ratios were both greater than 2 (Fig. 3C). The BxPC-3 tumor uptake of ^{99m}Tc-HHK was significantly inhibited (Figs. 3A and 3D) in the HK blocking group. ^{99m}Tc-HHK was unable to detect HEK293 tumors because of the negative expression of integrin $\alpha_v\beta_6$ in this tumor. For direct comparison, the ^{18}F-FDG PET scan of the same mice was obtained before the ^{99m}Tc-HHK scan. As shown in Figure 3B, all of the tumors in the 3 groups can be clearly visualized by ^{18}F-FDG PET. The accumulation of

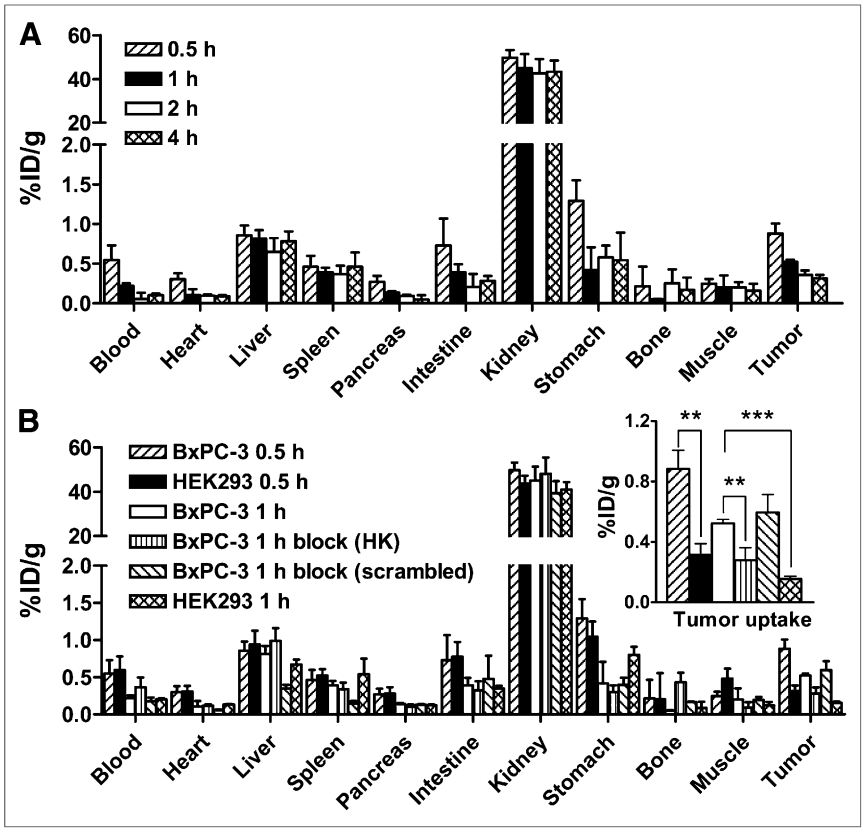

FIGURE 2. (A) Biodistribution of ^{99m}Tc-HHK in BxPC-3 tumor–bearing nude mice at 0.5, 1, 2, and 4 h after injection. (B) Biodistribution of ^{99m}Tc-HHK in BxPC-3 and HEK293 tumor–bearing nude mice at 0.5 and 1 h after injection and in BxPC-3 tumor–bearing nude mice coinjected with cold HK peptide or with scrambled peptide as blocking agent at 1 h after injection. Inset: ^{99m}Tc-HHK tumor uptake values from B. $^{**}P < 0.01$. $^{***}P < 0.001$.

^{18}F-FDG activity in the integrin $\alpha_v\beta_6$–positive BxPC-3 (with and without cold HK peptide blocking) and integrin $\alpha_v\beta_6$–negative HEK293 tumors was not significantly different (Fig. 3E).

Small-Animal SPECT/CT Imaging

As shown in Figure 4A, a liver metastatic BxPC-3 tumor lesion was clearly detected by ^{99m}Tc-HHK with high contrast in the abdominal region of the mouse. Supplemental Video 1 better shows the in vivo pharmacokinetics and tumor-targeting efficiency of ^{99m}Tc-HHK at 1 h after injection. After SPECT imaging, the mouse was sacrificed, and the presence of the well-established tumor growth in the liver was verified by anatomic visualization after dissection. The liver showed an extensive tumor burden (Figs. 4B and 4C) in the mouse that had a positive ^{99m}Tc-HHK imaging signal (Fig. 4A). The H&E staining results of the dissected tumor lesion further confirmed the ^{99m}Tc-HHK SPECT/CT findings (Fig. 4D).

DISCUSSION

Accumulated evidence shows the vital function of integrin $\alpha_v\beta_6$ in cancer progression, invasion, and metastasis. Integrin $\alpha_v\beta_6$ is significantly upregulated in many carcinomas, including approximately 100% of pancreatic cancers, whereas it is undetectable or is not expressed in the corresponding normal tissues (*3*). Blockade of integrin $\alpha_v\beta_6$ by a specific antibody inhibits tumor progression in animal models (*20*). Thus, integrin $\alpha_v\beta_6$ is a promising biomarker for cancer diagnosis and therapy. Consequently, several peptides and antibodies have been developed for integrin $\alpha_v\beta_6$ targeting.

A high-affinity 20-mer peptide antagonist (TP H2009.1) of integrin $\alpha_v\beta_6$ was previously developed by phage display (*13,15*). The integrin $\alpha_v\beta_6$–binding region of the 20-mer peptide is the DLXXL motif (*21*), where X indicates a nonspecific amino acid. This region is also conserved in many other integrin $\alpha_v\beta_6$–targeting ligands (*7–10,22,23*). We synthesized a SPECT radiotracer (^{99m}Tc-HHK) based on the TP H2009.1 peptide and evaluated the potential of this radiotracer in integrin $\alpha_v\beta_6$–targeted cancer detection. Using the integrin $\alpha_v\beta_6$–positive BxPC-3 cell line (Fig. 1A), we found that introduction of the HYNIC chelator to the HK peptide did not significantly affect receptor binding (Fig. 1B). Similar to that of ^{125}I-HYK, the binding of ^{99m}Tc-HHK on integrin $\alpha_v\beta_6$–positive BxPC-3 cells also exhibited a dose-dependent inhibition in the presence of cold HK peptide, and the IC_{50} value was calculated to be 0.65 ± 0.15 nM (Supplemental Fig. 2). Taken together, in vitro studies suggest that ^{99m}Tc-HHK maintains high receptor-binding affinity and specificity and could thus be tested for in vivo applications.

The in vivo integrin $\alpha_v\beta_6$–binding specificity of ^{99m}Tc-HHK was clearly demonstrated by the biodistribution and imaging studies. ^{99m}Tc-HHK showed rapid tumor accumulation in the BxPC-3 tumor model, and the radiotracer showed maximum tumor uptake values at 0.5 h after injection. As predicted, ^{99m}Tc-HHK uptake in the integrin $\alpha_v\beta_6$–negative HEK293 tumors remained close to background levels. Moreover, the tumor uptake of ^{99m}Tc-HHK was almost completely blocked by the coinjection of excess HK peptide (integrin $\alpha_v\beta_6$–specific (*15*)) but not by the coinjection of excess scrambled peptide (integrin $\alpha_v\beta_6$–nonspecific) (Fig. 2). These results further confirm that the tumor location is receptor-mediated. ^{99m}Tc-HHK was relatively stable in human serum in vitro (Supplemental Fig. 3). However, the metabolism study indicated that it was nearly completely metabolized in the blood, kidneys, and urine at 1 h after injection (Supplemental Fig. 4). These results are consistent with those of other studies on linear peptide-based radiotracers (*24,25*). The metabolic instability of ^{99m}Tc-HHK possibly contributes partially to its rapid clearance from tumor and normal organs. The metabolized small fractions of the radiotracer were cleared mainly via the renal route, which may be the main reason for the high kidney uptake. Although the absolute tumor uptake of ^{99m}Tc-HHK was relatively low (<1 %ID/g), the radiotracer was also rapidly cleared from nontargeting normal organs. As a result, the specific tumor targeting of ^{99m}Tc-HHK resulted in favorable tumor-to-nontumor ratios and tumor imaging contrast. The imaging study clearly demonstrated that the BxPC-3 pancreatic cancer xenografts can be visualized with high contrast using ^{99m}Tc-HHK, and the integrin $\alpha_v\beta_6$ expression was confirmed by ex vivo immunofluorescence staining (Supplemental Fig. 5).

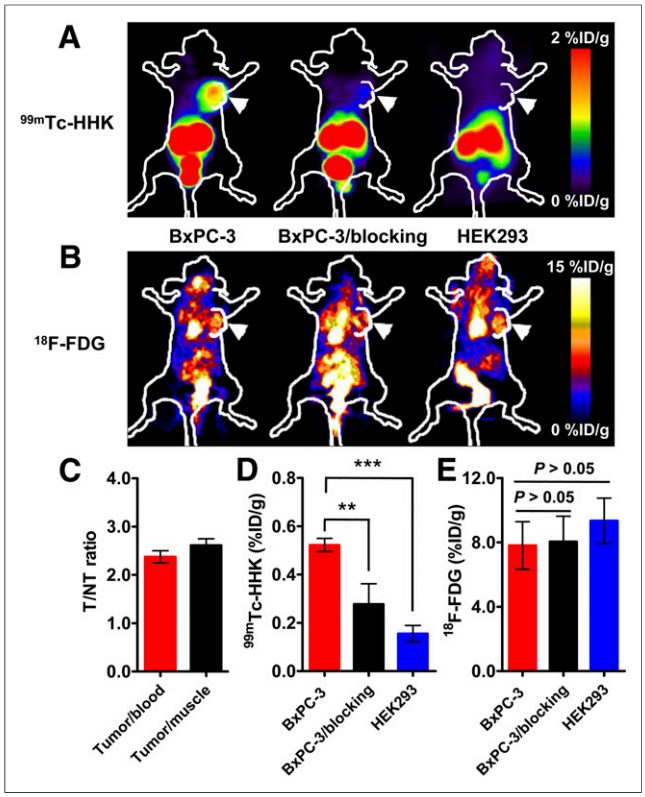

FIGURE 3. (A–B) Representative planar γ (A) and small-animal PET (B) images obtained at 1 h after injection of ^{99m}Tc-HHK or ^{18}F-FDG in BxPC-3 and HEK293 tumor–bearing mice without or with blocking dose of cold HK peptide. Arrows indicate tumor location. (C) Tumor-to-blood and tumor-to-muscle ratios of ^{99m}Tc-HHK at 1 h after injection of ^{99m}Tc-HHK in BxPC-3 tumor–bearing mice. (D–E) Comparison of tumor uptake of ^{99m}Tc-HHK (D) and ^{18}F-FDG (E) in BxPC-3 tumors, HEK293 tumors, and BxPC-3 tumors (cold HK peptide blocking) at 1 h after injection. $^{**}P < 0.01$. $^{***}P < 0.001$.

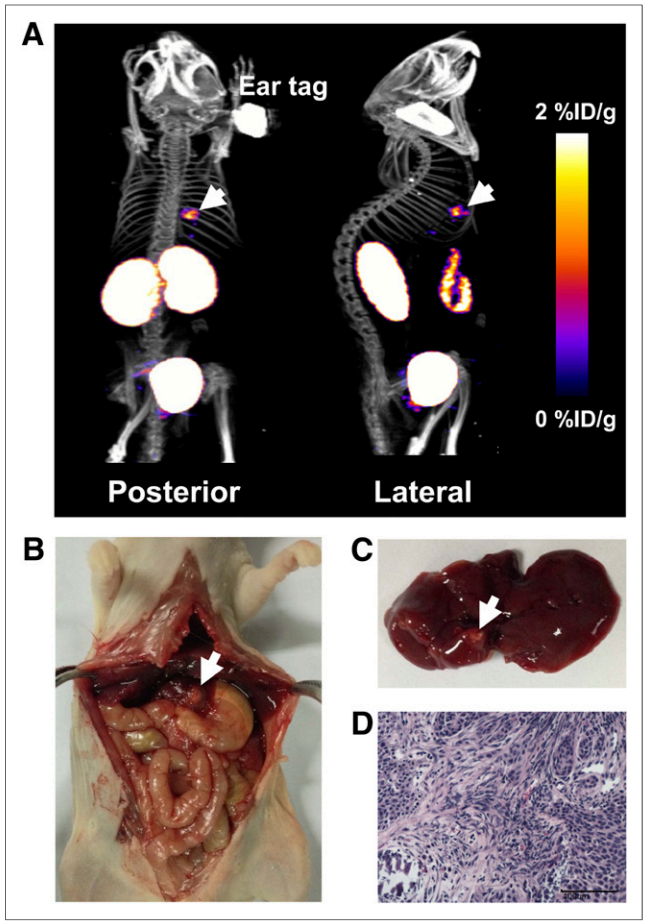

FIGURE 4. (A) Representative whole-body posterior and right lateral NanoSPECT/CT images of nude mice with liver metastasis of BxPC-3 tumors obtained at 1 h after ^{99m}Tc-HHK injection. (B) Mouse from A was sacrificed and dissected to verify liver metastasis. (C) Gross picture of liver from B. Metastatic liver lesions are indicated by white arrows. (D) H&E staining of metastatic liver tumor.

^{18}F-FDG is currently the most commonly used radiotracer for cancer detection and monitoring of treatment efficacy in clinical settings. However, ^{18}F-FDG is not tumor receptor–specific. ^{99m}Tc-HHK failed to detect tumors in the integrin $\alpha_v\beta_6$–blockade and integrin $\alpha_v\beta_6$–negative tumor models. By contrast, ^{18}F-FDG PET was unable to differentiate between tumors with integrin $\alpha_v\beta_6$ expression and those without such expression. These results demonstrate that ^{99m}Tc-HHK SPECT is superior to ^{18}F-FDG PET for the noninvasive imaging of integrin $\alpha_v\beta_6$ expression during tumor growth and for monitoring changes in integrin $\alpha_v\beta_6$ levels after anticancer treatment.

SPECT/CT imaging combines the high sensitivity of SPECT and the high spatial resolution of CT and provides both anatomic and functional information on the imaged cancer tissue. Metastasis to the liver is a common clinical finding for advanced pancreatic cancer (*26,27*); thus, we determined the performance of ^{99m}Tc-HHK SPECT/CT in the noninvasive detection of liver metastasis of pancreatic cancer using high-sensitivity and high-resolution small-animal SPECT/CT imaging. The high-resolution CT scan provides anatomic information, whereas SPECT imaging with ^{99m}Tc-HHK provides the integrin $\alpha_v\beta_6$ expression level of the metastasis. SPECT/CT imaging allows the identification and localization of small metastatic liver lesions (<5 mm in diameter) with high sensitivity and accuracy (Fig. 4), suggesting that ^{99m}Tc-HHK–based SPECT/CT has potential applications in many clinical scenarios, including early detection of small metastatic lesions and noninvasive imaging of residual or recurrent lesions after cancer surgery. The liver metastatic model used in this study is that of late-stage metastatic formation. The early stages of pancreatic cancer metastasis, such as local invasion at the primary lesion site and local lymphatic metastasis, are bypassed by direct injection of pancreatic tumor cells into the liver. Future studies using more suitable models of early spontaneous metastatic formation phases may further validate the capability of ^{99m}Tc-HHK for integrin $\alpha_v\beta_6$–targeted detection of early pancreatic cancer metastasis.

Compared with other integrin $\alpha_v\beta_6$–targeting radiotracers, ^{99m}Tc-HHK is more readily available (Supplemental Table 1). The high labeling yield of ^{99m}Tc-HHK allows the formulation of kits that can be extensively used in preclinical and clinical applications. However, a major drawback of ^{99m}Tc-HHK is its relatively low tumor uptake, which may be partly due to its in vivo metabolic instability. Optimization strategies (e.g., cyclization, PEGylation, and multimerization) (*28*) that have been successfully used to modify Arg-Gly-Asp (RGD)–based radiotracers may be required to further increase the receptor-binding affinity and improve the in vivo pharmacokinetics of ^{99m}Tc-HHK. With improved in vivo behaviors, the integrin

$\alpha_v\beta_6$–targeted SPECT tracer may be used in clinical trials for cancer screening, micrometastasis detection, and treatment monitoring.

CONCLUSION

^{99m}Tc-HHK exhibited specific integrin $\alpha_v\beta_6$ binding both in vitro and in vivo. ^{99m}Tc-HHK was successfully used in the specific detection of subcutaneous pancreatic tumor xenografts and liver metastases. Further optimization of ^{99m}Tc-HHK may eventually yield a suitable radiotracer for the detection of integrin $\alpha_v\beta_6$–positive tumors and for monitoring of the receptor expression during integrin $\alpha_v\beta_6$–targeted cancer treatment in clinical settings.

DISCLOSURE

The costs of publication of this article were defrayed in part by the payment of page charges. Therefore, and solely to indicate this fact, this article is hereby marked "advertisement" in accordance with 18 USC section 1734. This work was supported by National Natural Science Foundation of China (NSFC) projects (81222019, 81125011, 81000625, 81201127, 81321003, and 81230051), "973" projects (2013CB733802 and 2011CB707705), grants from the Ministry of Science and Technology of China (2011YQ030114, 2012ZX09102301-018, and 2012BAK25B03-16), grants from the Ministry of Education of China (31300 and BMU20110263), grants from the Beijing Natural Science Foundation (7132131 and 7132123), and a grant from the Beijing Nova Program (Z121107002512010). No other potential conflict of interest relevant to this article was reported.

REFERENCES

1. Siegel R, Naishadham D, Jemal A. Cancer statistics, 2013. *CA Cancer J Clin.* 2013;63:11–30.
2. Mendieta Zerón H, Garcia Flores JR, Romero Prieto ML. Limitations in improving detection of pancreatic adenocarcinoma. *Future Oncol.* 2009;5:657–668.
3. Bandyopadhyay A, Raghavan S. Defining the role of integrin $\alpha_v\beta_6$ in cancer. *Curr Drug Targets.* 2009;10:645–652.
4. Sipos B, Hahn D, Carceller A, et al. Immunohistochemical screening for beta6-integrin subunit expression in adenocarcinomas using a novel monoclonal antibody reveals strong up-regulation in pancreatic ductal adenocarcinomas in vivo and in vitro. *Histopathology.* 2004;45:226–236.
5. Bates RC, Bellovin DI, Brown C, et al. Transcriptional activation of integrin beta6 during the epithelial-mesenchymal transition defines a novel prognostic indicator of aggressive colon carcinoma. *J Clin Invest.* 2005;115:339–347.
6. Hazelbag S, Kenter GG, Gorter A, et al. Overexpression of the $\alpha_v\beta_6$ integrin in cervical squamous cell carcinoma is a prognostic factor for decreased survival. *J Pathol.* 2007;212:316–324.
7. Hausner SH, DiCara D, Marik J, Marshall JF, Sutcliffe JL. Use of a peptide derived from foot-and-mouth disease virus for the noninvasive imaging of human cancer: generation and evaluation of 4-[^{18}F]fluorobenzoyl A20FMDV2 for in vivo imaging of integrin $\alpha_v\beta_6$ expression with positron emission tomography. *Cancer Res.* 2007;67:7833–7840.
8. Hausner SH, Abbey CK, Bold RJ, et al. Targeted in vivo imaging of integrin $\alpha_v\beta_6$ with an improved radiotracer and its relevance in a pancreatic tumor model. *Cancer Res.* 2009;69:5843–5850.
9. Kimura RH, Teed R, Hackel BJ, et al. Pharmacokinetically stabilized cystine knot peptides that bind alpha-v-beta-6 integrin with single-digit nanomolar affinities for detection of pancreatic cancer. *Clin Cancer Res.* 2012;18:839–849.
10. Hackel BJ, Kimura RH, Miao Z, et al. ^{18}F-fluorobenzoate-labeled cystine knot peptides for PET imaging of integrin $\alpha_v\beta_6$. *J Nucl Med.* 2013;54:1101–1105.
11. Wadas TJ, Wong EH, Weisman GR, Anderson CJ. Copper chelation chemistry and its role in copper radiopharmaceuticals. *Curr Pharm Des.* 2007;13:3–16.
12. Jia B, Liu Z, Zhu Z, et al. Blood clearance kinetics, biodistribution, and radiation dosimetry of a kit-formulated integrin $\alpha_v\beta_6$-selective radiotracer ^{99m}Tc-3PRGD2 in non-human primates. *Mol Imaging Biol.* 2011;13:730–736.
13. Oyama T, Sykes KF, Samli KN, Minna JD, Johnston SA, Brown KC. Isolation of lung tumor specific peptides from a random peptide library: generation of diagnostic and cell-targeting reagents. *Cancer Lett.* 2003;202:219–230.
14. Zhou X, Chang YC, Oyama T, McGuire MJ, Brown KC. Cell-specific delivery of a chemotherapeutic to lung cancer cells. *J Am Chem Soc.* 2004;126:15656–15657.
15. Elayadi AN, Samli KN, Prudkin L, et al. A peptide selected by biopanning identifies the integrin $\alpha_v\beta_6$ as a prognostic biomarker for nonsmall cell lung cancer. *Cancer Res.* 2007;67:5889–5895.
16. Liu Z, Jia B, Shi J, et al. Tumor uptake of the RGD dimeric probe ^{99m}Tc-G3-2P4-RGD2 is correlated with integrin $\alpha_v\beta_3$ expressed on both tumor cells and neovasculature. *Bioconjug Chem.* 2010;21:548–555.
17. Liu Z, Huang J, Dong C, et al. ^{99m}Tc-labeled RGD-BBN peptide for small-animal SPECT/CT of lung carcinoma. *Mol Pharm.* 2012;9:1409–1417.
18. Yang ZF, Ho DW, Ng MN, et al. Significance of CD90$^+$ cancer stem cells in human liver cancer. *Cancer Cell.* 2008;13:153–166.
19. Liu Z, Jin C, Yu Z, et al. Radioimmunotherapy of human colon cancer xenografts with ^{131}I-labeled anti-CEA monoclonal antibody. *Bioconjug Chem.* 2010;21:314–318.
20. Van Aarsen LA, Leone DR, Ho S, et al. Antibody-mediated blockade of integrin $\alpha_v\beta_6$ inhibits tumor progression in vivo by a transforming growth factor-beta-regulated mechanism. *Cancer Res.* 2008;68:561–570.
21. Kraft S, Diefenbach B, Mehta R, Jonczyk A, Luckenbach GA, Goodman SL. Definition of an unexpected ligand recognition motif for $\alpha_v\beta_6$ integrin. *J Biol Chem.* 1999;274:1979–1985.
22. Nothelfer EM, Zitzmann-Kolbe S, Garcia-Boy R, et al. Identification and characterization of a peptide with affinity to head and neck cancer. *J Nucl Med.* 2009;50:426–434.
23. Saha A, Ellison D, Thomas GJ, et al. High-resolution in vivo imaging of breast cancer by targeting the pro-invasive integrin $\alpha_v\beta_6$. *J Pathol.* 2010;222:52–63.
24. Shi J, Jia B, Liu Z, et al. ^{99m}Tc-labeled bombesin(7-14)NH_2 with favorable properties for SPECT imaging of colon cancer. *Bioconjug Chem.* 2008;19:1170–1178.
25. Harris TD, Sworin M, Williams N, et al. Synthesis of stable hydrazones of a hydrazinonicotinyl-modified peptide for the preparation of ^{99m}Tc-labeled radiopharmaceuticals. *Bioconjug Chem.* 1999;10:808–814.
26. Yamada H, Hirano S, Tanaka E, Shichinohe T, Kondo S. Surgical treatment of liver metastases from pancreatic cancer. *HPB (Oxford).* 2006;8:85–88.
27. Ouyang H, Wang P, Meng Z, et al. Multimodality treatment of pancreatic cancer with liver metastases using chemotherapy, radiation therapy, and/or Chinese herbal medicine. *Pancreas.* 2011;40:120–125.
28. Liu S. Radiolabeled multimeric cyclic RGD peptides as integrin $\alpha_v\beta_3$ targeted radiotracers for tumor imaging. *Mol Pharm.* 2006;3:472–487.

JNM The Journal of NUCLEAR MEDICINE

Integrin $\alpha_v\beta_6$–Targeted SPECT Imaging for Pancreatic Cancer Detection

Zhaofei Liu, Hao Liu, Teng Ma, Xianlei Sun, Jiyun Shi, Bing Jia, Yi Sun, Jun Zhan, Hongquan Zhang, Zhaohui Zhu and Fan Wang

J Nucl Med. 2014;55:989-994.
Published online: April 7, 2014.
Doi: 10.2967/jnumed.113.132969

The Journal of Nuclear Medicine is published monthly.
SNMMI | Society of Nuclear Medicine and Molecular Imaging
1850 Samuel Morse Drive, Reston, VA 20190.
(Print ISSN: 0161-5505, Online ISSN: 2159-662X)

SNMMI SOCIETY OF NUCLEAR MEDICINE AND MOLECULAR IMAGING